PAPER

Check for updates

Exploring non-covalent interactions in excited states: beyond aromatic excimer models†

Ariel C. Jones and Lars Goerigk *

Time-dependent density functional theory (TD-DFT) offers a relatively accurate and inexpensive approach for excited state calculations. However, conventional TD-DFT may suffer from the same poor description of non-covalent interactions (NCIs) which is known from ground-state DFT. In this work we present a comprehensive benchmark study of TD-DFT for excited-state NCIs. This is achieved by calculating dissociation curves for excited complexes ('exciplexes'), whose binding strength depends on excited-state NCIs including electrostatics, Pauli repulsion, charge-transfer, and London dispersion. Reference dissociation curves are calculated with the reasonably accurate wave function method SCS-CC2/CBS(3,4) which is used to benchmark a range of TD-DFT methods. Additionally, we test the effect of ground-state dispersion corrections, DFT-D3(BJ) and VV10, for exciplex binding. Overall, we find that TD-DFT methods generally under-bind exciplexes which can be explained by the missing dispersion forces. Underbinding errors reduce going up the rungs of Jacob's ladder. Further, the D3(BJ) dispersion correction is essential for good accuracy in most cases. Likewise, the VV10-type non-local kernel yields relatively low errors and has comparable performance in either its fully self-consistent implementation or as a post-SCF additive correction, but its impact is solely on ground-state energies and not on excitation energies. From our analysis, the most robust TD-DFT methods for exciplexes with localised excitations in their equilibrium and non-equilibrium geometries are the double hybrids B2GP-PLYP-D3(BJ) and B2PLYP-D3(BJ). Their range-separated versions ωB2(GP-)PLYP-D3(BJ) or the spin-opposite scaled, range-separated double hybrid SOS-ωB88PP86 can be recommended when charge transfer plays a role in the excitations. We also identify the need for a state-specific dispersion correction as the next step for improved TD-DFT performance.

1 Introduction

Linear-response time-dependent density functional theory (TD-DFT) in the adiabatic approximation has become the method of choice for excited-state computational chemistry.[1,2] TD-DFT offers reasonable accuracy at a relatively low computational cost which makes it feasible to study chemical systems of interest (up to around 100 atoms). Within the adiabatic approximation, the exchange–correlation kernel is time-independent and is therefore known from ground state DFT.[3,4] As such, it could be expected that TD-DFT calculations suffer from the same pitfalls as the underlying density functional approximation (DFA).

It is well-established that common DFAs fail to correctly account for the London dispersion force[5] which is a long-range electron correlation effect, whereas pure DFT correlation is (semi)-local.[6–8] Comprehensive ground-state benchmark studies have demonstrated that properly accounting for non-covalent interactions (NCIs), particularly dispersion forces, is essential for good computational accuracy, including for barrier heights, reaction energies, and geometries.[9–14] Nonetheless, the performance of TD-DFT methods for excited-state NCIs remains significantly undertested.[15]

TD-DFT benchmarking studies have primarily focused on single chromophores and their excited-state properties, including vertical transition energies,[16–23] oscillator strengths,[16,24] electronic circular dichroism,[24–26] and UV-vis spectra,[24,27] among others. The most robust methods generally belong to the time-dependent double hybrid density functional approximations (TD-DHDFAs).[20,21,28,29] Generalised gradient approximation (GGA) and meta-GGA methods systematically redshift excitation energies and furthermore produce low-lying 'ghost' excitations which are not observed in experimental spectra.[17,19,30,31] Hybrid methods, particularly with a large proportion of Fock exchange, reduce this redshift although can in turn lead to blueshifted excitations.[18,19,26,30] Global TD-DFT

School of Chemistry, The University of Melbourne, Parkville, Australia.
E-mail: lars.goerigk@unimelb.edu.au; Tel: +61-3-83446784

† Electronic supplementary information (ESI) available: Details for CBS extrapolation, values for D_e and r_e, dissociation curves, styrene-TMA excitation energies, more details on ALMO-EDA, CT statistics, mean absolute errors, optimised geometries and geometries used to generate dissociation curves. See DOI: https://doi.org/10.1039/d4cp03214d

25192 | *Phys. Chem. Chem. Phys.*, 2024, **26**, 25192–25207

This journal is © the Owner Societies 2024

methods fail to describe long-range excitations—Rydberg and charge-transfer (CT)—for which range-separation (RS) is required.[20,31-35] TD-DHDFAs have been shown to describe exciton coupling in dimers.[15,36]

Excited-state NCIs have been investigated in the context of excited complexes known as 'exciplexes'—or 'excimers' when both monomers are identical—which are more strongly bound when in their excited state compared to their ground state counterpart.[37] Exciplex and excimer studies have been more thoroughly reviewed previously.[15] These studies have generally tested a small number of TD-DFT methods and/or chemical systems.[38-41] Typical studies that systematically tested ground-state dispersion corrections relied on the older DFT-D2[42] approach.[40,41] Some authors have adjusted dispersion corrections specifically for excited-state complexes,[41,43] again limited to a small number of DFAs and chemical systems. Nonetheless, improved performance is generally observed when either a ground-state or state-specific dispersion correction is applied.

Recently, Hancock and Goerigk performed a comprehensive benchmarking study of excited-state NCIs for aromatic excimers[15] which was later[44] expanded to test spin-component scaled[45] (SCS) and spin-opposite scaled[46] (SOS) TD-DHDFAs.[29,47] It was shown that the smallest errors are achieved by spin-scaled RS double-hybrid methods. An additive ground-state dispersion correction generally reduced the error of TD-DFT methods although was inadequate to fully capture the excited-state dispersion forces in aromatic excimers. This strongly suggests the need to develop an excited-state dispersion correction.

However, before this endeavour can be undertaken, benchmark-quality data is needed to gain further insights into the current state-of-the art methods and allow for future training and cross-validation of any new excited-state specific dispersion corrections. Hence, this work aims to expand the currently limited benchmarking data on excited-state NCIs. We test a number of exciplexes—benzene–neon, benzene–argon, benzene–naphthalene, toluene–tetracyanoethylene (TCNE), and styrene–trimethylamine (TMA) (Fig. 1)—which range from dispersion-dominated exciplexes to those with a significant CT component.

Benzene-rare gas dimers have previously been explored by DFT in the ground state.[8,48,49] However, as far as we are aware, this is the first time that TD-DFT methods have been applied to the benzene–neon and benzene–argon exciplexes. A small number of studies have used TD-DFT methods to investigate NCIs in benzene–naphthalene,[39] toluene–TCNE,[50] and styrene-TMA exciplexes.[40] These studies employed a conservative number of DFAs and dispersion corrections either were not systematically tested or were neglected entirely. We build on these findings by testing a large number of TD-DFT methods, which include RS methods and double-hybrid DFAs, for five exciplexes.

Additionally, we present the first study of TD-SCS/SOS-DHDFAs for these exciplexes, namely with the 14 functionals presented by Casanova-Páez and Goerigk in 2021,[29] which have shown promising performance for single chromophore excitations.[29,51] Recently, these functionals were defined for their ground-state energy which has allowed their use for aromatic excimer interaction energies.[44] In this study, we test these methods for new exciplexes beyond the aromatic dimers.

Furthermore, we systematically assess the performance of ground-state dispersion corrections when applied to exciplexes. This includes Grimme's additive dispersion correction DFT-D3(BJ)[52,53] with Becke–Johnson damping. This correction adds the missing dispersion energy by an atom-pairwise summation:

$$E_{\text{disp}}^{\text{DFT-D3(BJ)}} = -\frac{1}{2} \sum_{A \neq B} \sum_{n=6,8} s_n \frac{C_n^{AB}}{R_{AB}^n + (a_1 R_{BJ}^{AB} + a_2)^n}, \quad (1)$$

where C_n^{AB} is the dispersion coefficient for atom pair AB. These coefficients depend on the chemical environment of atoms A and B and are calculated on the fly from pre-tabulated ground-state dynamic polarizabilities. Dividing by R^n enforces the correct R^{-6} decay for long-range dispersion forces and R^{-8} covers the medium range. R_{BJ}^{AB} is damping-function specific and calculated from C_n^{AB}. The factor s_6 is set to unity for most DFAs except for DHDFAs; see ref. 54 for details on how it is determined. s_8, as well as parameters $a_{1/2}$ in the damping function, are fitted for each DFA.

An alternative ground-state dispersion correction is van der Waals DFT (vdW-DFT) which incorporates non-local correlation into the DFA.[55] As such, the dispersion force has an explicit dependence on electron density which is not the case for additive DFT-D approaches. Vydrov and Van Voorhis' VV10 method[56] is currently the most popular vdW-DFT approach which shows promising accuracy. Hujo and Grimme were the first to generalise non-local DFT (DFT-NL),[57] in which the VV10 non-local correlation kernel can be used to augment an existing DFA as per eqn (2).
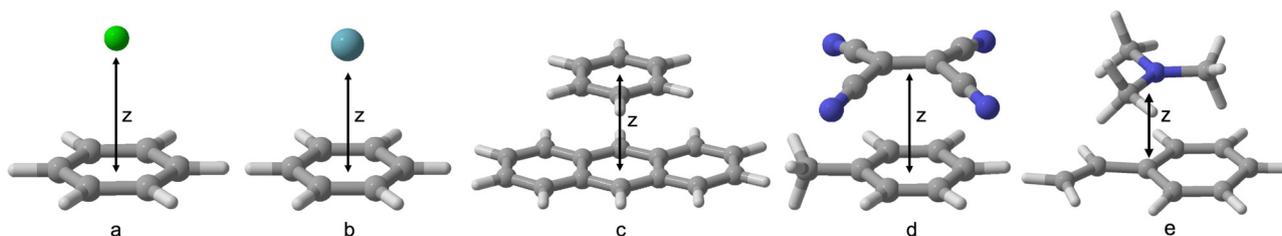

Fig. 1 Benchmarked exciplexes with dissociation coordinate z: (a) benzene–neon; (b) benzene–argon; (c) benzene–naphthalene; (d) toluene–TCNE; (e) styrene–trimethylamine.

This journal is © the Owner Societies 2024

Phys. Chem. Chem. Phys., 2024, **26**, 25192–25207 | **25193**

DFT-NL requires the fitting of a single parameter b to ensure a seamless connection to the short-range DFA.

$$E_{XC}^{DFT\text{-}NL} = E_X^{DFT} + E_C^{DFT} + E_C^{VV10} \qquad (2)$$

The DFT-NL approach is appealing in that it attempts to solve the dispersion issue at the DFA level. However, it has been shown that when VV10 non-local correlation is implemented in a post-SCF fashion, this yields highly comparable accuracy to the self-consistent implementation.[57,58] We assess for the first time DFT-NL in the context of excited state NCIs, including both the self-consistent and post-SCF forms. We also assess other VV10-based vdW-DFT functionals that have shown good performance when tested for thermochemistry[13] and on the extensive GMTKN55 test set.[10,59]

This study aims to expand the benchmarking data for excited-state NCIs. Specifically, we present the first comprehensive benchmarking study for exciplexes including those with significant CT character. We benchmark 38 TD-DFT methods, among which include some of the currently most accurate methods for excited state properties such as the recently developed TD-SCS/SOS-DHDFAs. Furthermore, we test the effect of the ground-state dispersion correction when applied to exciplex binding.

2 Computational details

Geometry optimisations were performed for all exciplexes in their lowest-lying singlet excited state, calculated at the second-order approximate coupled-cluster (CC2) level of theory[60] in its SCS form[61] and with the def2-TZVP[62] triple-ζ atomic orbital (AO) basis set. Dissociation curves were generated by freezing the internal coordinates and translating monomers along the z-coordinate shown in Fig. 1. 65 geometries were obtained per dimer, with z ranging from 2 Å to 16 Å and with the greatest density of geometries about the equilibrium distance. Interaction energies were defined relative to the energy at 16 Å, where the monomers are sufficiently non-interacting. At the dissociation limit only one monomer is excited while the other remains in its electronic ground state.

Reference dissociation curves were calculated for each exciplex in its lowest-lying singlet excited state. These calculations were performed at the SCS-CC2 level of theory with a triple-ζ quadruple-ζ (TZ-QZ) complete basis set (CBS) extrapolation. The CBS extrapolation procedure has been previously described in ref. 15, see ESI† for details. The authors additionally showed that this method provides suitably accurate reference data for excimer binding of small to moderately sized systems. We ran additional tests to confirm its suitability and refer the reader to Section 1 of the ESI.†

Benchmarking dissociation curves were calculated for the TD-DFT methods shown in Table 1, also for the lowest-lying singlet excitation. Where the D3(BJ) correction has been parameterised for a given method, D3(BJ) dispersion energies were calculated using the DFTD3 V3.1 standalone program.[63] All TD-DFT benchmarking used the def2-QZVP basis set, except for the

Table 1 TD-DFT methods benchmarked, classified according to rungs on Jacob's ladder;[66] citations are provided for the methods and the studies that determined their dispersion correction parameters

ORCA 5.0.3	TURBOMOLE 7.4.1	QCHEM 6.0.1
	GGA	
	BLYP$^{a\,53,67-69}$	
	PBE$^{a\,53,70}$	
	BP86$^{a\,53,67,71}$	
	meta-GGA	
		B97M-V^{72}
	Hybrid	
	Global	
	B3LYP$^{a\,53,73,74}$	
	BHLYP$^{a\,14,75}$	
	PBE0$^{a\,53,76,77}$	
	Range-separated	
LC-BLYP^{78}	CAM-B3LYP$^{a\,14,79}$	ωB97X-V^{80}
LC-PBE^{81}	ωB97X^{82}	ωB97M-V^{83}
ωB97X-D3(BJ)$^{ab\,58,80}$		
	Double hybrid	
	Global	
B2GP-PLYP$^{a\,14,84}$		
SCS-B2GP-PLYP$^{a\,29,44}$		
SOS-B2GP-PLYP$^{a\,29,44}$		
B2PLYP$^{a\,14,85}$		
SOS-B2PLYP$^{a\,29,44}$		
PBE-QIDH$^{a\,86,87}$		
SCS-PBE-QIDH$^{a\,29,44}$		
SOS-PBE-QIDH$^{a\,29,44}$		
PBE0-DH$^{a\,88,89}$		
	Range-separated	
RSX-0DH$^{a\,59,90}$		
RSX-QIDH$^{a\,59,91}$		
SCS-RSX-QIDH$^{a\,29,44}$		
SOS-RSX-QIDH$^{ac\,29,44}$		
ωB2GP-PLYP$^{a\,20,59}$		
SCS-ωB2GP-PLYP$^{a\,29,44}$		
SOS-ωB2GP-PLYP$^{a\,29,44}$		
ωB2PLYP$^{a\,20,59}$		
SOS-ωB2PLYP$^{a\,29,44}$		
ωB88PP86$^{a\,29,44}$		
SCS-ωB88PP86$^{a\,29,44}$		
SOS-ωB88PP86$^{a\,29,44}$		
ωPBEPP86$^{a\,29,44}$		
SCS-ωPBEPP86$^{a\,29,44}$		
SOS-ωPBEPP86$^{a\,29,44}$		

^{a} D3(BJ) correction has been parameterised for this method. ^{b} The D3(BJ) correction replaces the VV10 kernel of the ωB97X-V functional.[58] ^{c} Not to be confused with SOS-RSX-QIDH or SOS1-RSX-QIDH as presented later in ref. 92 and 93.

benzene–neon exciplex which required the decontracted def2-QZVP basis set to obtain the correct dissociation curves in ORCA 5.0.3.[64,65] Testing revealed that decontracted def2-QZVP resulted in the same well-depth and position of the minimum compared to this basis set in its contracted form; however, the larger decontracted basis set was needed to produce smooth curves that otherwise suffered from numerical noise.

SCS-CC2 calculations were performed with TURBOMOLE 7.4.1[94] and TD-DFT calculations were performed using TURBOMOLE 7.4.1, ORCA 5.0.3,[64,65] or QCHEM 6.0.1[95] as per Table 1. To obtain total energies for TD-SCS/SOS-DHDFAs, additional

keywords had to be added to the ORCA inputs, as outlined in ref. 44. All calculations in TURBOMOLE and ORCA used the resolution of the identity (RI) approximation with the appropriate auxiliary basis sets.[62,96] In ORCA, calculations additionally used the COSX approximation for exchange integrals.[97] For all double-hybrid calculations, the RI approximation[98,99] was applied to the (SCS/SOS-)MP2 ground state term and excited-state (SCS/SOS-) configuration interaction singles with perturbative doubles [CIS(D)] terms.[100,101] The same approximation was also used in all SCS-CC2 calculations.

The RI approximation was not used in QCHEM TD-DFT calculations due to a technical issue with its parallel implementation on the National Computational Infrastructure. Nonetheless, it was found that the RI approximation resulted in essentially no change to the calculated interaction energy.

Additionally, the frozen core approximation was applied throughout, for which the chemical-core definition was chosen. The SCF convergence threshold for all calculations was $10^{-7}\ E_{\text{h}}$, and in QCHEM THRESH was set to $10^{-12}\ E_{\text{h}}$. Calculations used the grid options 'defgrid2' for ORCA and gridsize 7 for TURBO-MOLE. QCHEM calculations required a large unpruned integration grid containing 99 radial points and 590 angular points. The default SG-1 grid was used for VV10 non-local correlation in QCHEM where applicable.

Dissociation curves were analysed in terms of their minimum values. A cubic interpolation was used between each point on the dissociation curve, resulting in a finely interpolated curve containing 14 000 points from which the minimum was located with a resolution of 0.001 Å. The dissociation energy (D_{e}) is defined as the negative interaction energy at the minimum. The equilibrium distance (r_{e}) is the distance between monomers at the minimum, in terms of the coordinate z (Fig. 1). Where the TD-DFT method predicts an entirely repulsive dissociation curve (*i.e.* all positive interaction energies with no minimum), D_{e} has been estimated as the negative interaction energy at the reference r_{e} distance. In these cases, no r_{e} for the method is reported and the D_{e} is negative.

3 Results and discussion

In this section, we first present the calculated dissociation curves for each exciplex categorised into those with a localised or CT excitation. The following discussion primarily concerns the calculated D_{e} which is of greater chemical relevance than r_{e}. For simplicity and given the large number of methods tested, complete dissociation curves for TD-SCS/SOS-DHDFAs are provided in the ESI† and discussed generally in Section 3.3. Likewise for the D3(BJ) dispersion-corrected methods which are discussed in Section 3.4.1. Additionally, all values for D_{e} and r_{e} are provided in the ESI.† We then discuss the physical origins for exciplex binding and verify the nature of the excitation (localised or CT) based on orbital analysis and an Energy Decomposition Analysis (EDA) in Section 3.5. Finally, the averaged results for all DFAs are presented in Section 3.6.

3.1 Benchmarking exciplexes with localised excitations

3.1.1 Benzene-rare gas exciplexes. The dissociation curves are shown for the benzene–neon exciplex in Fig. 2 and for the benzene–argon exciplex in Fig. 3. In both cases, the first excitations are localised on benzene. The reference D_{e} and r_{e} are respectively: 0.29 kcal mol^{-1} and 3.44 Å for benzene–neon; and 1.07 kcal mol^{-1} and 3.49 Å for benzene–argon. The relatively weak interaction energies are unsurprising for these small, dispersion-dominated systems and the stronger binding for benzene–argon can be attributed to its greater number of electrons.

For both exciplexes, GGA (panel A in the two figures) and global hybrid methods (both panels B, continuous lines) tend to underestimate D_{e}. Some of these DFAs show entirely repulsive dissociation curves and fail to predict exciplex formation, which are BLYP, BP86, and B3LYP. Underbinding can be attributed to the known limitation of GGA and hybrid methods for describing dispersion forces. Of the GGA methods tested, only PBE correctly predicts an attractive D_{e} for both the benzene-rare gas exciplexes. This aligns with the established
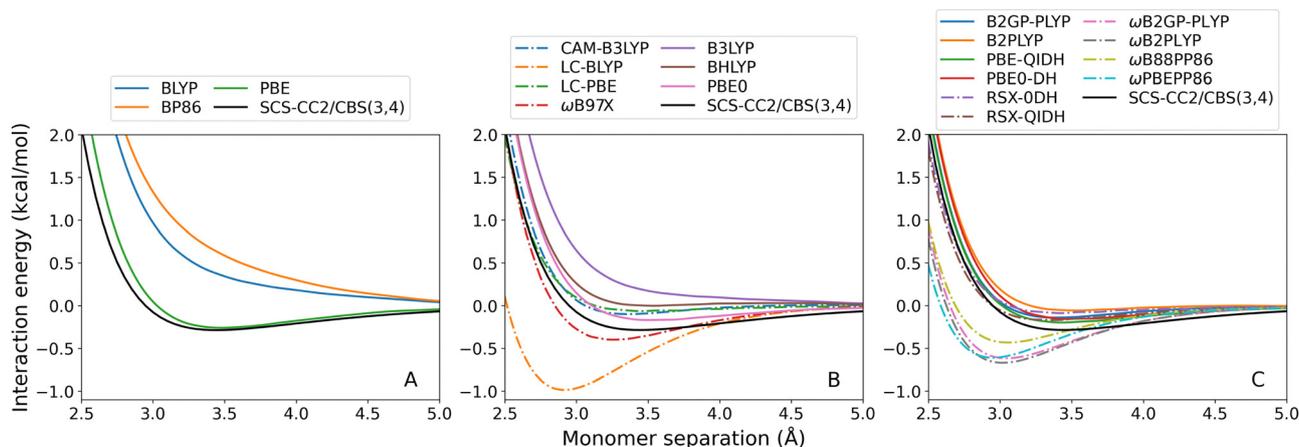

Fig. 2 Benzene–neon TD-DFT dissociation curves, calculated for the lowest-lying singlet excited state. From left to right: (A) GGA; (B) hybrid; and (C) double-hybrid DFAs. Range-separated methods are indicated by dash-dotted lines.
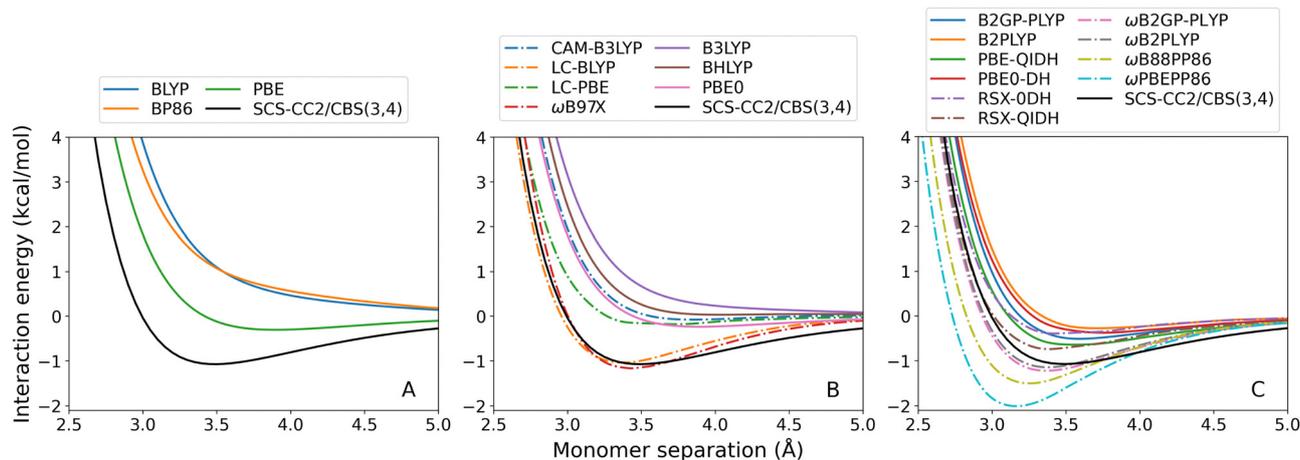
This journal is © the Owner Societies 2024

Phys. Chem. Chem. Phys., 2024, **26**, 25192–25207 | **25195**

Fig. 3 Benzene–argon TD-DFT dissociation curves, calculated for the lowest-lying singlet excited state. From left to right: (A) GGA; (B) hybrid; and (C) double-hybrid DFAs. Range-separated methods are indicated by dash-dotted lines.

trend that PBE shows partially attractive behaviour when describing ground-state NCIs.[42,102–104]

The observed underbinding is improved with the inclusion of range-separation (panels B and C in both figures, dash-dotted lines): however; this results in overbinding for a number of dispersion-uncorrected RS methods (LC-BLYP, ωB97X, ωB2PLYP, ωB2GP-PLYP, ωB88PP86, and ωPBEPP86). CAM-B3LYP is barely attractive with D_e = 0.08 kcal mol^{-1} for benzene–argon and D_e = 0.10 kcal mol^{-1} for benzene–neon. While the global double-hybrid DFAs show the most consistent performance, interestingly these do not comprise the best methods for the benzene-rare gas exciplexes. Surprisingly, dispersion-uncorrected PBE is the best-performing method for benzene–neon in terms of the D_e error which is only 0.03 kcal mol^{-1}. PBE-QIDH has the next best result for this exciplex, with 0.09 kcal mol^{-1} error. For benzene–argon, three DFAs have errors below the 0.1 kcal mol^{-1} chemical accuracy threshold for NCIs. These are: LC-BLYP (0.04 kcal mol^{-1});

ωB2PLYP (0.07 kcal mol^{-1}); and ωB97X (0.09 kcal mol^{-1}). PBE does not perform as well for the argon system as for the neon one.

3.1.2 Benzene–anthracene exciplex. Fig. 4 shows the benzene–anthracene exciplex dissociation curves. The reference D_e is 7.79 kcal mol^{-1} and r_e is 3.35 Å. This larger binding strength is shown to arise from electrostatics and some CT stabilisation which is discussed in Section 3.5.

As previously observed for the benzene-rare gas exciplexes, GGA (Fig. 4(A)) and global hybrid (Fig. 4(B), continuous lines) DFAs systematically underbind the benzene–anthracene exciplex. Both BLYP and BP86 predict entirely repulsive dissociation curves, and the D_e error for PBE is large (7.51 kcal mol^{-1}). Of the global hybrids, only PBE0 predicts a positive D_e however also with a large error of 7.70 kcal mol^{-1}. The benzene–anthracene exciplex is also under-bound by the RS hybrids (Fig. 4(B), dash-dotted lines), global double-hybrids (Fig. 4(C), continuous lines), and most of the RS double-hybrids (Fig. 4(C), dash-dotted lines), which was not the case for the benzene-rare gas
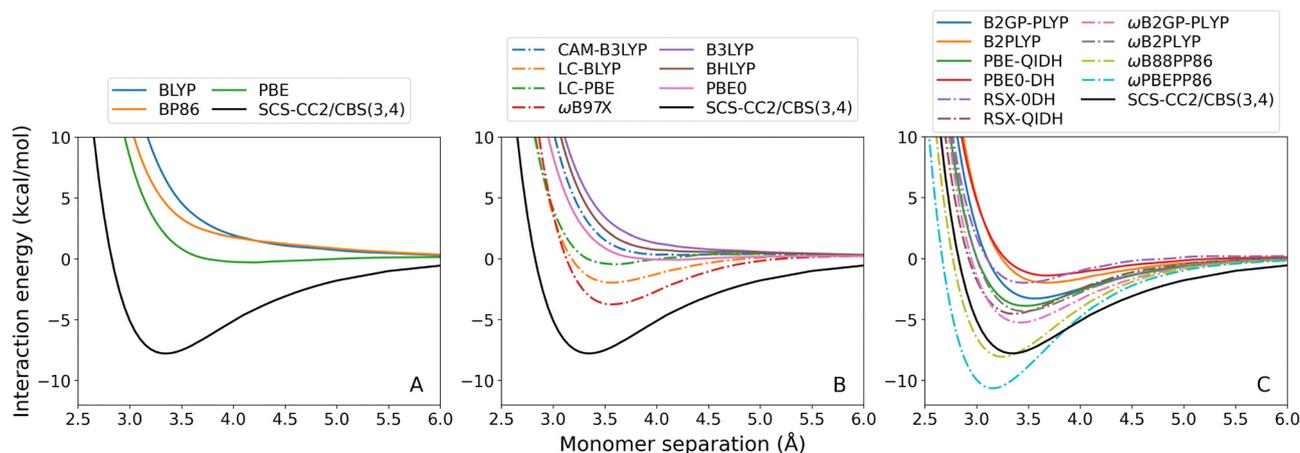

Fig. 4 Benzene–anthracene TD-DFT dissociation curves, calculated for the lowest-lying singlet excited state. From left to right: (A) GGA; (B) hybrid; and (C) double-hybrid DFAs. Range-separated methods are indicated by dash-dotted lines.

25196 | *Phys. Chem. Chem. Phys.*, 2024, **26**, 25192–25207

This journal is © the Owner Societies 2024

exciplexes. CAM-B3LYP yields a purely repulsive curve with an unusual inflection point at 4.91 Å.

As before, ωB88PP86 and ωPBEPP86 overestimate D_e for this exciplex. Nonetheless, ωB88PP86 has the smallest absolute error for benzene–anthracene which is 0.27 kcal mol^{-1} compared to the reference. Of the methods that do not over-bind this exciplex, ωB2GP-PLYP has the smallest error which is 2.54 kcal mol^{-1}. None of the dispersion-uncorrected DFAs tested are able to reproduce D_e within the 0.1 kcal mol^{-1} chemical accuracy threshold. However, for ωB88PP86 the error comprises only 3% of the total binding energy.

3.1.3 Toluene–TCNE exciplex (3A′). For toluene–TCNE, the lowest-lying singlet state is an unphysical CT excitation at the 16 Å dissociation limit when calculated with SCS-CC2/def2-QZVP. As such, the second excited state (overall the third A′ state and herein referred to as 3A′) has also been calculated which has the correct excitation at the dissociation limit and only involves excitation on TCNE (Fig. S15, ESI†). The dissociation curves for the 3A′ state are shown in Fig. 5. The reference D_e is 12.37 kcal mol^{-1} and r_e is 3.26 Å.

For toluene–TCNE 3A′, the dispersion-uncorrected methods again systematically underbind this exciplex with the exception of ωB88PP86 and ωPBEPP86 which over-bind every tested exciplex. Unlike for previous exciplexes, every GGA and global hybrid method correctly predicts a positive (attractive) binding strength for toluene–TCNE 3A′. Nonetheless, these methods have large errors ranging from 8.00 to 11.17 kcal mol^{-1} for the GGAs (Fig. 5(A)) and from 7.16 to 9.43 kcal mol^{-1} for the global hybrid methods (Fig. 5(B), continuous lines). An unusual feature of this system is that the GGA methods fail to capture the correct underlying shape of the dissociation curves, instead appearing with a sharp elbow about the calculated minima.

Underbinding persists for the RS methods (dash-dotted lines in Fig. 5(B)) and double-hybrid methods (Fig. 5(C)), although errors in D_e are generally reduced. For toluene-TCNE 3A′, the DFA with the closest agreement for D_e is ωB2GP-PLYP with 0.78 kcal mol^{-1} error. While this is not within the chemical accuracy limit, this represents a reasonably small 6% error.

3.2 Benchmarking exciplexes with CT transitions

3.2.1 Toluene–TCNE CT excitation (2A′). For technical reasons, the toluene–TCNE 3A′ state has been presented previously because this results in the correct energy at the dissociation limit. The toluene–TCNE 3A′ state is a localised excitation while the first singlet excitation (overall the second A′ state, herein referred to as 2A′) has strong CT character (see Section 3.5). It is therefore of interest to analyse the 2A′ state, despite its incorrect energy at the dissociation limit, in order to benchmark TD-DFT methods for dimers with CT excitations. The excitation involves the highest occupied molecular orbital (HOMO), which is localised on toluene, and the lowest unoccupied molecular orbital (LUMO), which is localised on TCNE (Fig. S15, ESI†). The toluene–TCNE dissociation curves for the 2A′ CT state are shown in Fig. 6. From the SCS-CC2/CBS(3,4) reference, D_e is 49.68 kcal mol^{-1} and r_e is 3.17 Å.

None of the GGA methods were able to calculate correct dissociation curves for the 2A′ state. This reflects the inherent limitation of GGA methods, which contain only semi-local DFT exchange, for calculating long-range excitations.[31] Of the global hybrids (panel A, continuous lines) only BHLYP correctly predicts dimer formation however shows severe under-binding. Correspondingly, the calculated r_e is far too large with an error of 0.74 Å (23%). Notably, the performance of the hybrid functionals directly correlates with the proportion of Fock exchange they contain: 20% for B3LYP, which is the worst-performing global hybrid; 25% for PBE0; and 50% for BHLYP, which is the best-performing global hybrid. The global double-hybrid methods (panel B, continuous lines) again reduce exciplex underbinding although with particularly large errors in D_e ranging from 19.87 to 31.46 kcal mol^{-1}.

For both the hybrid and double-hybrid methods, RS (dash-dotted lines) greatly improves the calculated D_e and r_e which is unsurprising given the importance of long-range Fock
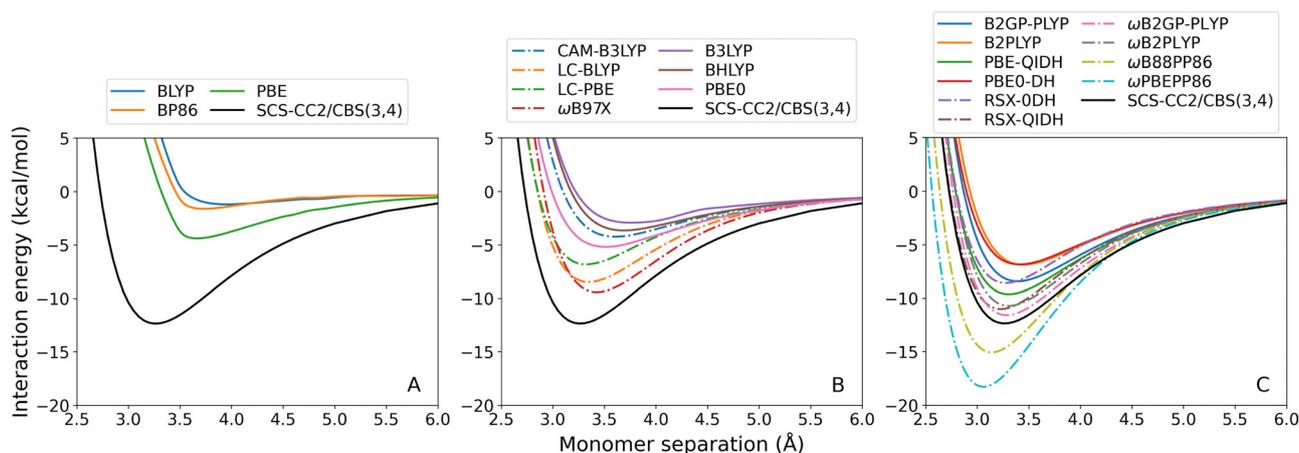

Fig. 5 Toluene−TCNE TD-DFT dissociation curves for the second singlet excited state 3A′. From left to right: (A) GGA; (B) hybrid; and (C) double−hybrid DFAs. Range-separated methods are indicated by dash-dotted lines.
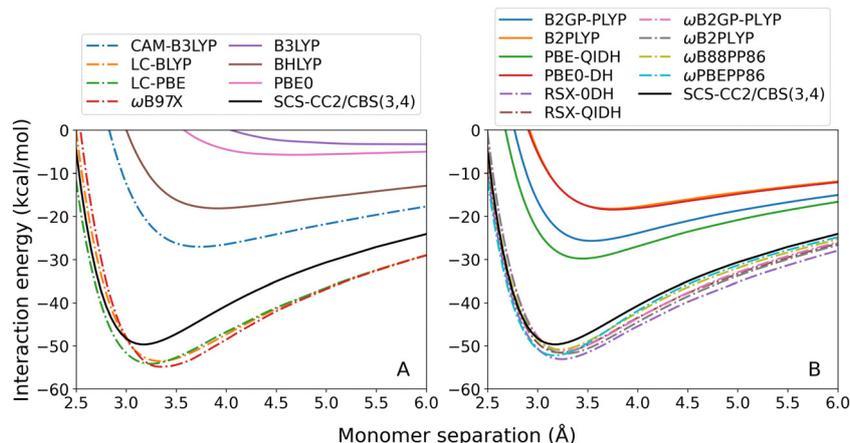
This journal is © the Owner Societies 2024

Phys. Chem. Chem. Phys., 2024, **26**, 25192–25207 | **25197**

Fig. 6 Toluene−TCNE TD-DFT dissociation curves for the first singlet excited state 2A′. From left to right: (A) hybrid; and (B) double-hybrid DFAs. Range-separated methods are indicated by dash-dotted lines.

exchange for describing CT excitations. However, with the exception of CAM-B3LYP, this results in an over-correction that leads to over-binding. Nonetheless, the lowest absolute error is given by ωB88PP86 which over-estimates D_e by 1.20 kcal mol^{-1} (2% error).

3.2.2 Styrene-TMA exciplex. Styrene-TMA is another challenging exciplex with CT character. For this exciplex at its equilibrium geometry, the lowest-lying singlet state is a CT excitation. On the other hand, the dissociated monomers show an excitation localised on styrene. Every TD-DFT method correctly predicts the CT excitation at short distances, but all fail to calculate the correct excitation for the dissociated monomers at 16 Å. To generate dissociation curves, the TD-DFT energies were calculated as normal between 2 Å and 6 Å. The correct endpoint energy was calculated from the isolated monomers (ground-state TMA plus excited-state styrene). The resulting dissociation curves are shown in Fig. 7 and the reference values are 28.79 kcal mol^{-1} for D_e and 3.01 Å for r_e.

The styrene-TMA dissociation curves show the opposite trend in that all TD-DFT methods over-bind this exciplex.

This over-binding can be attributed to strongly redshifted excitations at the minimum which is a CT excitation, whereas this redshift is less pronounced or becomes a blueshift at the endpoint which has a localised excitation. This imbalance leads to an artificially lowered minimum in the interaction energy curves due to the total energies of the minimum structures being too low and the interaction energies being the differences between total energies. Examples for select DFAs are shown in Table 2. GGA methods, which show the most pronounced over-binding and the largest redshifts near their respective minima at 3 Å, underestimate SCS-CC2/def2-QZVP energies by about 2 eV. This redshift is reduced with the inclusion of Fock exchange, and in particular for RS methods. Excitation energies for all assessed DFAs are shown in the ESI† (Section 4.2).

The GGA methods (Fig. 7(A)) have particularly large errors in D_e ranging from 57.00 to 62.94 kcal mol^{-1}. The double-hybrid and RS methods show improvements compared to the other methods. In particular, RS is needed for a more accurate treatment of this CT excitation. The RS double-hybrid methods (7C, dash-dotted lines) generally show the most robust performance,
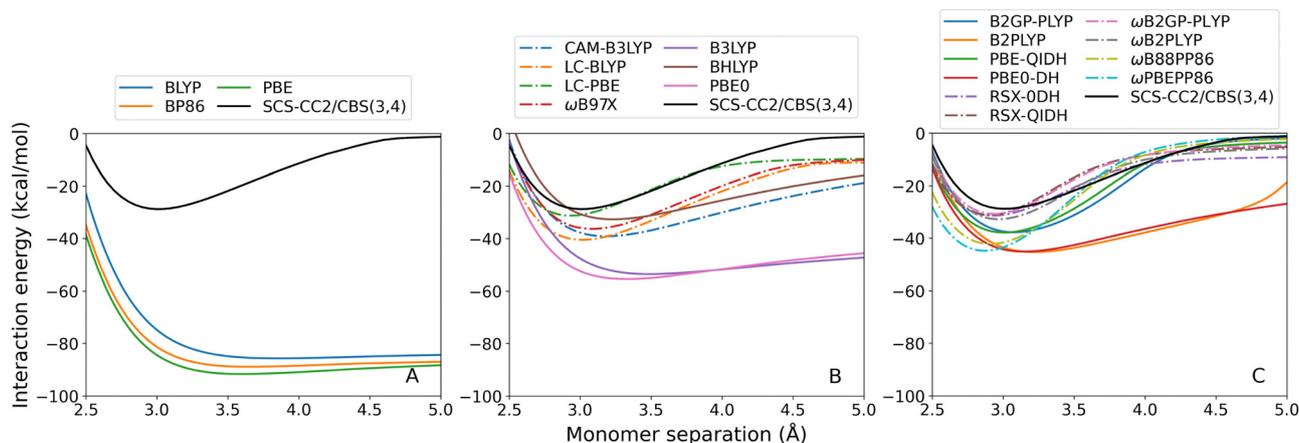

Fig. 7 Styrene-TMA TD-DFT dissociation curves, calculated for the lowest-lying singlet excited state. From left to right: (A) GGA; (B) hybrid; and (C) double-hybrid DFAs. Range-separated methods are indicated by dash-dotted lines.

25198 | *Phys. Chem. Chem. Phys.*, 2024, **26**, 25192–25207

This journal is © the Owner Societies 2024

Table 2 Deviations in eV from SCS-CC2/def2-QZVP excitation energies for the styrene–TMA 2A′ transition near the equilibrium distance (3 Å) and at the 16 Å dissociation endpoint for select methods. A negative deviation stands for redshifted excitation energies relative to the reference

DFA	Deviation (eV)	
	3 Å	16 Å
BP86	−2.10	0.58
PBE	−2.13	0.58
BLYP	−2.03	0.54
B3LYP	−1.26	0.04
BHLYP	−0.07	0.42
CAM-B3LYP	−0.41	0.31
ωB97X	0.02	0.43
SOS-ωB2PLYP	0.10	0.00

with the exception of ωB88PP86 and ωPBEPP86. The best performance is achieved by ωB2GP-PLYP with 1.92 kcal mol^{-1} absolute error in D_e.

3.3 Spin-scaled double-hybrid methods

Fourteen TD-SCS/SOS-DHDFAs have been recently developed for the calculation of excitation energies.[29] They have then been extended to also define their ground-state total energies, which allows the calculation of interaction energies for excited states.[44] These methods were tested for the exciplexes in the current study. For brevity, the complete dissociation curves are given in the ESI† and examples of typical SCS/SOS results are shown in Fig. 8 for the toluene–TCNE localised 3A′ excitation.

With the exception of SCS-RSX-QIDH, spin-scaling (both SCS and SOS) consistently reduces the binding strength predicted for all exciplexes. This is unsurprising given the small scaling parameters fitted for the SCS and SOS methods, which results in reduced non-local correlation compared to the unscaled methods.[29,44] Of the spin-scaled methods, SOS methods generally predict weaker binding although in some cases the SCS and SOS methods calculate virtually identical results. This can again be rationalised by the similar parameterisation between SCS and SOS variants. For example, parameter fitting for both B2PLYP and ωB2PLYP leads to SCS results that are identical to the SOS fit (*i.e.* no same-spin contribution and identical opposite-spin scaling). Indeed, all of the SCS methods have

small or negligible contributions to their same-spin term with the only exception being SCS-RSX-QIDH. As a result, SCS-RSX-QIDH shows the reverse trend in which this method calculates stronger exciplex binding compared to unscaled RSX-QIDH.

The overall effect of TD-SCS/SOS-DHDFAs is both method- and system-dependent. Where the unscaled functional already demonstrates under-binding, this is exacerbated by spin-scaling (*e.g.* Fig. 8(A)). However for methods that overestimate D_e, the SCS and SOS methods yield improved performance (*e.g.* Fig. 8(B)). The only exception is for SCS-RSX-QIDH which shows the opposite trend in that SCS improves under-binding (*e.g.* Fig. 8(C)) or exacerbates over-binding. Generally, ωB88PP86 and ωPBEPP86 show the greatest improvements by spin-scaled methods. These methods have a large MP2 contribution and consistently over-bind the tested exciplexes, and as such their improved behaviour with SCS/SOS is unsurprising.

3.4 Effect of ground-state dispersion correction

3.4.1 DFT-D3(BJ) correction. The effect of the additive D3(BJ) dispersion correction has been systematically tested across all exciplexes for the applicable DFAs, including all TD-SCS/SOS-DHDFAs for their recent D3(BJ) fits.[44] Other DFT-D variants were not considered as these have been shown to give similar results to D3(BJ) in the case of DFT-D4[105,106] for excimer binding[15] and for both DFT-D4 and DFT-D3 zero-damping[52] when tested on the GMTKN55 test set.[59] Given the large number of DFAs tested, the complete D3(BJ)-corrected dissociation curves are given in the (ESI†). Fig. 9 shows the exciplex dissociation curves calculated with D3(BJ)-corrected global hybrid DFAs as a representative example.

Unsurprisingly, the D3(BJ) correction was found to increase the binding strength predicted by almost every DFA which results in a larger D_e and shorter r_e. In some cases, the dispersion-uncorrected DFA failed entirely to predict exciplex formation (for example, the benzene-rare gas dimers calculated with B3LYP shown in Fig. 9) which is generally fixed by the D3(BJ) correction. A notable exception is that D3(BJ) makes little or negligible difference to the binding strength predicted by RS TD-DHDFAs, including their SCS/SOS variants. This has
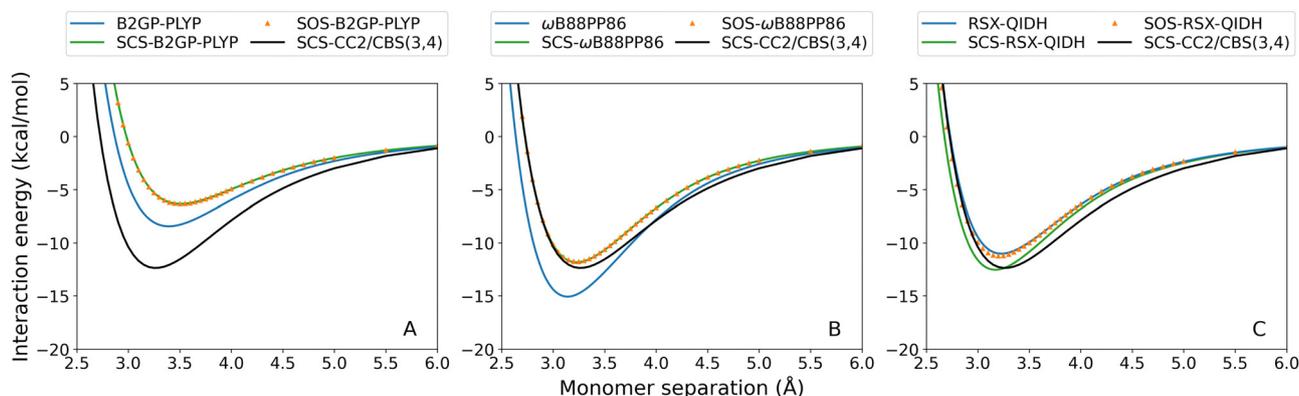

Fig. 8 Toluene−TCNE 3A′ dissociation curves for representative TD-DHDFAs and their SCS/SOS variants: (A) B2GP-PLYP; (B) ωB88PP86; (C) RSX-QIDH.

This journal is © the Owner Societies 2024

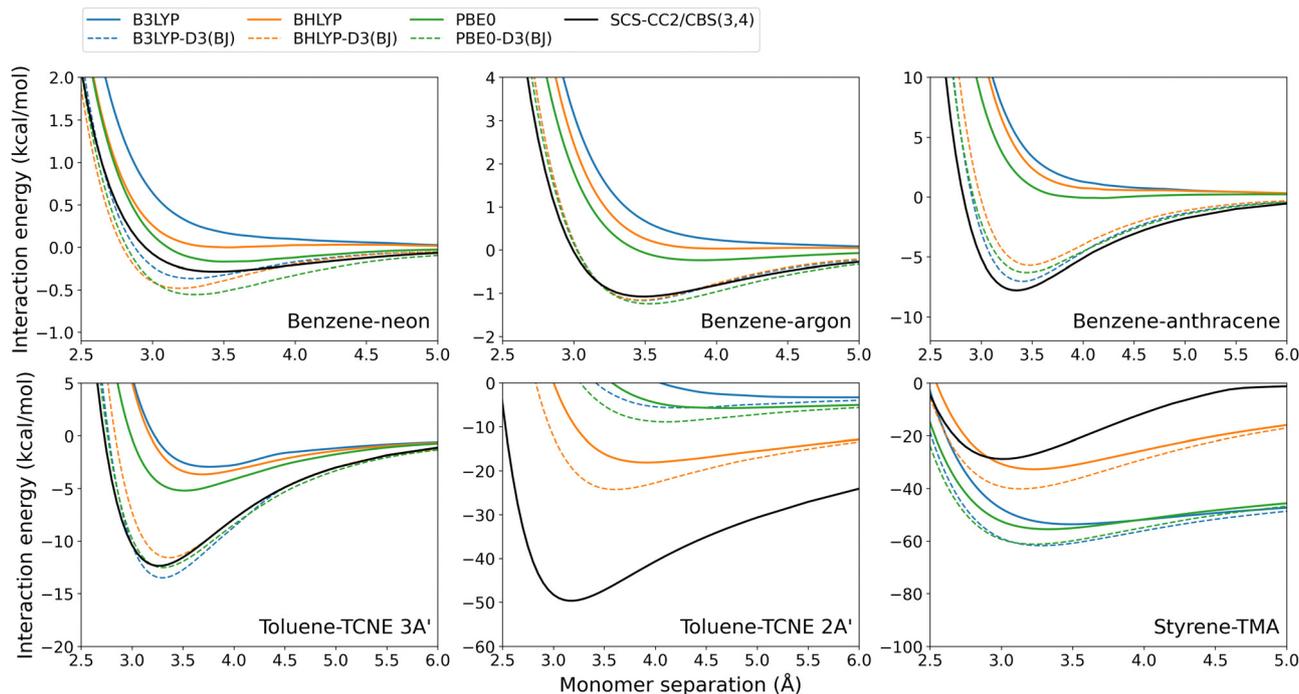*Phys. Chem. Chem. Phys.*, 2024, **26**, 25192–25207 | **25199**

Fig. 9 Exciplex dissociation curves for global hybrid DFAs with and without the D3(BJ) dispersion correction.

been previously noted for excimer binding[15,44] and on the GMTKN55 test set.[59,107] The physical reason for this remains unclear however is unlikely to be a result of the fit set used for the damping parameters. A recent re-fit was performed for the D3(BJ) damping parameters on a larger fit set, for the RS double hybrid methods ωB2GP-PLYP, ωB2PLYP, and RSX-QIDH.[44] This refit made no difference when tested for exciplex binding (see Fig. S14, ESI†) as was also the case in the original excimer study.[44]

In general, D3(BJ) greatly improves the results for the DFAs and exciplexes tested herein, as is discussed in Section 3.6. Nonetheless, the performance of this correction depends on the method and system tested. The benzene-rare gas exciplexes, which have particularly weak binding, show reasonably good agreement for some dispersion-uncorrected DFAs. As such, D3(BJ) can result in an overcorrection with a predicted D_e that is larger than the reference, which is particularly so for benzene–neon. Despite this, D3(BJ) generally results in reduced absolute errors for these exciplexes. On the other hand, the larger benzene–anthracene and toluene–TCNE 3A′ exciplexes generally exhibit underbinding for the dispersion-uncorrected methods. Applying the D3(BJ)-correction leads to good agreement with the reference and greatly reduces the error for each DFA tested (not including the RS TD-DHDFAs as discussed above).

The CT exciplexes again proved challenging to model with dispersion-corrected methods. For toluene–TCNE 2A′, the global hybrid and global double-hybrid DFAs showed severe underbinding which could not be entirely compensated for by D3(BJ). The calculated D_e values remain significantly underestimated by up to 44 kcal mol^{-1} in the case of B3LYP-D3(BJ).

In contrast, the RS methods show much better agreement to the reference for toluene–TCNE 2A′. As such, these methods can result in over-binding when the D3(BJ) correction is added.

Styrene-TMA is the only exciplex which is systematically over-bound by the dispersion-uncorrected DFAs. As previously discussed in Section 3.2.2, this is due to the CT excitation at the equilibrium distance being strongly redshifted while at the dissociation limit this redshift decreases or becomes a blue-shift. This imbalance causes an artificial over-binding from dispersion-uncorrected DFAs. As such, adding the D3(BJ) dispersion correction, which is by definition attractive, exacerbates this over-binding. This reflects a limitation of the underlying DFA rather than the dispersion correction.

The exception to this is for spin-scaled TD-DHDFAs, specifically SOS-ωB2GP-PLYP, SCS-ωB2GP-PLYP, and SOS-ωB2PLYP. For these methods, spin-scaling counteracts the over-binding predicted by the plain DFA and as such the D3(BJ) correction can improve D_e (see Fig. S6, ESI†).

3.4.2 VV10 correction. To the best of our knowledge, this study is the first time that the VV10 correction, and more generally VV10-based vdW-DFT functionals, have been assessed for excited state NCIs. The performance of combinatorially-optimised functionals incorporating VV10 was tested for the meta-GGA B97M-V and for the RS hybrid methods ωB97X-V and ωB97M-V. The results are shown in Fig. 10. The toluene–TCNE dissociation curve for B97M-V could not be obtained as this method failed to predict the correct excitation at the 16 Å dissociation limit, for both the 2A′ and 3A′ states. Fig. 10 also shows the ωB97X-D3(BJ) results for comparison. This method contains the same exchange–correlation component as ωB97X-V, except that the VV10 non-local correlation kernel has been
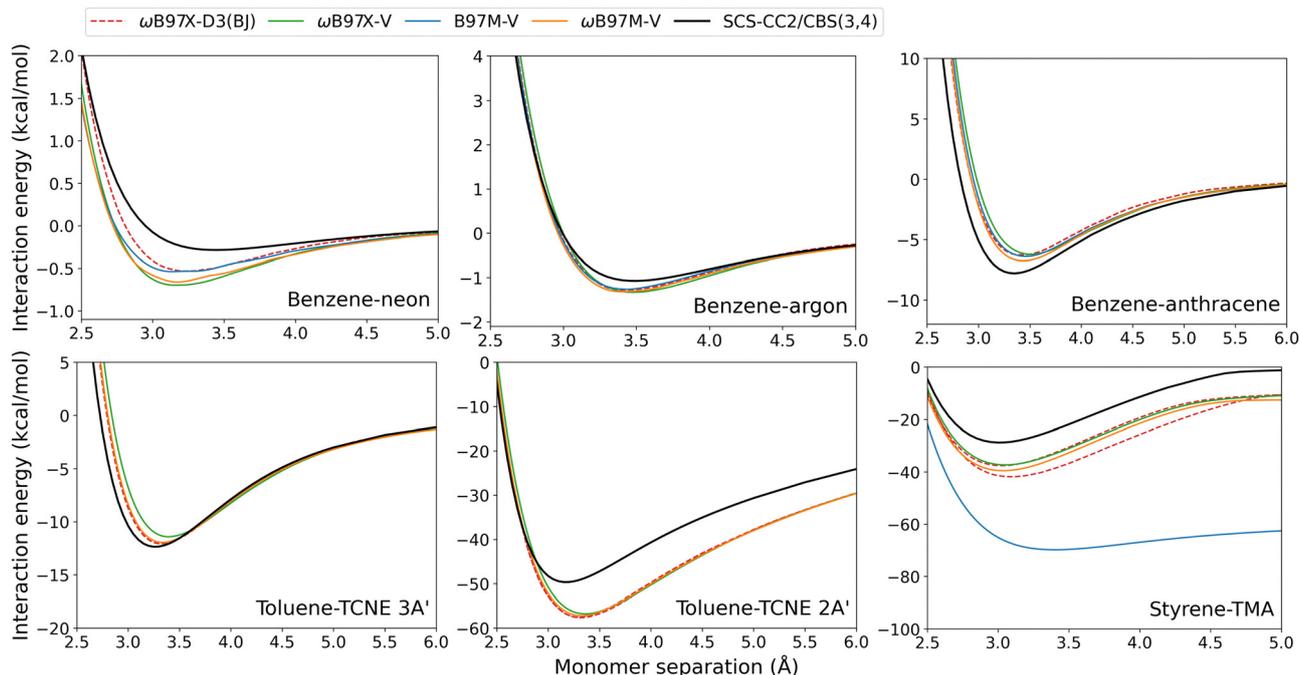
Fig. 10 Exciplex dissociation curves for combinatorially-optimised functionals with the VV10 dispersion correction. The ωB97X–D3(BJ) results are also shown for comparison.

removed and the D3(BJ) correction has been parameterisied for the underlying DFA.[58]

These VV10-corrected methods overbind both of the benzene–rare gas exciplexes and underbind benzene–anthracene and toluene–TCNE 3A′. This mirrors our observations made for the D3(BJ) correction. For these four exciplexes with localised excitations, D_e errors are reasonably small and range from: 0.19–1.40 kcal mol⁻¹ for B97M-V; 0.26–1.56 kcal mol⁻¹ for ωB97X-V; and 0.24–1.03 kcal mol⁻¹ for ωB97M-V. Interestingly, ωB97X–D3(BJ) slightly outperforms the original ωB97X-V functional for each of these four exciplexes.

The VV10-corrected methods show the greatest errors for the CT exciplexes. Toluene–TCNE 2A′ is over-bound by both ωB97X-V and ωB97M-V. In Section 3.2.1, it was shown that dispersion-uncorrected RS hybrid methods yield close agreement to the reference dissociation curve for toluene–TCNE 2A′. As such, this overbinding can be explained as an over-correction from VV10 dispersion. Styrene-TMA again shows overbinding by all of the VV10-corrected methods, especially for B97M-V which contains no Fock exchange. This overbinding is caused by a redshift in the CT excitation energy as described previously. The ωB97X–D3(BJ) and ωB97X-V functionals again show similar performance, although for these exciplexes ωB97X-V has slightly reduced errors.

Previous studies have shown that incorporating VV10 non-local correlation in a post-SCF fashion yields accuracies highly similar to self-consistent VV10.[57,58] Furthermore, the effect of VV10 on TD-DFT excitation energies was previously shown to be small. For example, the excitation energies of single chromophores were calculated with and without VV10 for the

functionals B97M-V, ωB97X-V, and ωB97M-V and the VV10 correction resulted in less than 0.01 eV change to the mean signed error.[18]

We tested two GGA functionals, BLYP and PBE, which were augmented with VV10 as per standard DFT-NL (eqn (2)) with values for b that were respectively 4.00[57] and 6.40.[108] The VV10 correction was implemented in three ways:

1. Self-consistent VV10 for the ground-state energy and VV10 included in the exchange–correlation kernel of the TD-DFT calculation.

2. Self-consistent VV10 for the ground-state energy and VV10 not included in the exchange–correlation kernel of the TD-DFT calculation.

3. Post-SCF VV10 correction for the ground-state energy and VV10 not included in the exchange–correlation kernel of the TD-DFT calculation.

These methods were tested for the benzene–argon exciplex as a case study and the results for D_e and r_e are shown in Table 3.

The calculated D_e and r_e show minimal change depending on how VV10 non-local correlation is implemented. For BLYP-NL, the difference in calculated binding energy is 0.04 kcal mol⁻¹ and for PBE-NL is only 0.01 kcal mol⁻¹ for post-SCF (C) *versus* fully self-consistent VV10 (A). The effect of VV10 on the calculated excitation energies is also small. This is reflected by the minimal change to D_e when VV10 is included fully self-consistently (A) compared to when only the ground-state energy is treated self-consistently and VV10 is not applied to the excitation energy (B).

For both BLYP-NL and PBE-NL, post-SCF VV10 (C) results in a smaller binding strength compared to when VV10 is included self-consistently (A). As a result, both of the post-SCF DFT-NL

This journal is © the Owner Societies 2024

Phys. Chem. Chem. Phys., 2024, **26**, 25192–25207 | **25201**

Table 3 D_e and r_e for DFT-NL methods with fully self-consistent or post-SCF VV10 implementation (see text for description of methods A–C), calculated for the benzene–argon exciplex. Results for the D3(BJ)-corrected methods are given for comparison

Method	D_e (kcal mol^{-1})	r_e (Å)
Reference	1.07	3.49
BLYP		
A	1.13	3.44
B	1.15	3.46
C	1.09	3.48
D3(BJ)	1.10	3.49
PBE		
A	1.41	3.48
B	1.42	3.48
C	1.40	3.46
D3(BJ)	1.27	3.49

Fig. 11 Stacked energy diagram of ALMO-EDA energies for exciplexes calculated with ωB97M-V/def2-TZVP.

methods have the best agreement to the reference due to a reduction in over-binding. PBE-D3(BJ) outperforms any of its VV10 counterparts. For BLYP, the best-performing method is BLYP-NL with post-SCF VV10 (C), although this is closely followed by BLYP-D3(BJ) which outperforms the self-consistent VV10 methods.

Overall, this case study supports that VV10 non-local correlation can be used post-SCF as an additive dispersion correction without loss of accuracy and at a lower computational cost.[57,58] Additionally, VV10 makes little difference to calculated excitation energies as previously reported by Head-Gordon and coworkers.[18] We further recommend that D3(BJ) can be used as an inexpensive dispersion correction which shows comparable accuracy to VV10.

3.5 Origin of exciplex binding strength

In this section, we provide an analysis of the physical origins for binding strength of the herein assessed dimers and verify the localised or CT nature of the excitations. An EDA scheme for exciplexes has been developed by Ge *et al.* which uses absolutely localised molecular orbitals (ALMO-EDA).[109] Exciplex interaction energy is decomposed into a frozen component, containing electrostatics and Pauli repulsion, energy from polarisation, and that from charge transfer (CT). The current scheme suffers from known limitations in that dispersion corrections contaminate the Pauli term and furthermore that the polarisation contribution is dependent on basis-set size.[109] Nonetheless, ALMO-EDA calculations have been performed for all exciplexes to qualitatively measure contributions to their binding strengths. These calculations were performed with ωB97M-V which has shown sufficiently accurate performance for each exciplex. The def2-TZVP basis set was used to balance the basis set superposition error with the polarisation issue known for ALMO-EDA. The ALMO-EDA results are shown in Fig. 11.

From Fig. 11, the ALMO-EDA calculations reproduce the correct qualitative trend for exciplex binding strength. The benzene-rare gas exciplexes have small dispersion-dominated interaction energies. For these exciplexes, their unphysically attractive Pauli energy is an artefact of ALMO-EDA wherein
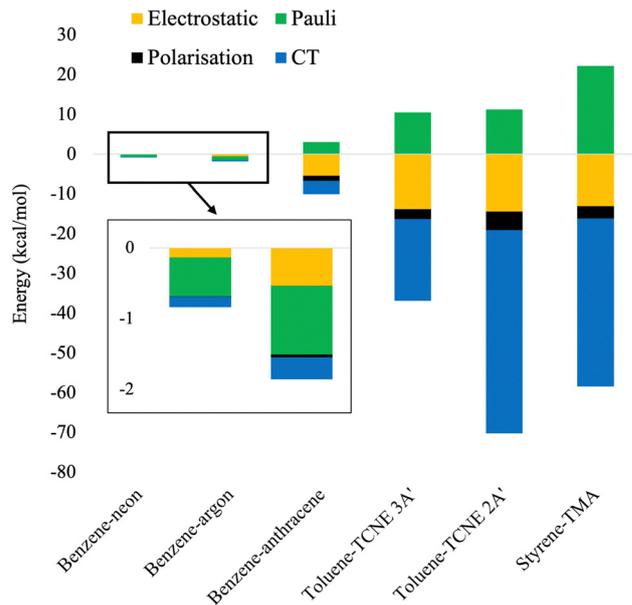
dispersion is included in this term. This contamination of the Pauli term has been noted in ref. 109 and which we further verified, see ESI† for details. Benzene–anthracene shows an overall larger binding strength which is significantly due to electrostatics and some CT nature. Toluene–TCNE 3A′ again has stronger binding and contains significant electrostatic and CT contributions. Finally, toluene–TCNE 2A′ and styrene-TMA have the largest binding strengths which are a result of their large CT components.

A different scheme for quantifying the CT nature of an excitation was developed by Plasser and Lischka, which uses the one-electron transition density matrix to calculate CT metrics.[110] In this scheme, the calculated CT number varies from 0 for entirely localised excitations to 1 for entirely charge-separated excitations. The calculated CT numbers, and additional CT metrics, are given in the ESI.† These calculated CT numbers generally complement the ALMO-EDA findings. The benzene-rare gas exciplexes have no CT character (CT number = 0) and the excitation is entirely localised on benzene. There is some CT quality for the benzene–anthracene exciplex (CT number = 0.04), although this is minimal and the excitation is primarily localised on anthracene. For toluene–TCNE, the 3A′ state has a small CT number of 0.04. This does not reflect the more significant CT component as predicted by ALMO-EDA although is consistent with the visualised molecular orbitals (MOs) for this transition (((HOMO−2)–LUMO excitation, Fig. S15, ESI†) which shows this excitation localised on the TCNE fragment. The CT number is 0.92 for toluene–TCNE 2A′ and is 0.83 for styrene-TMA, which confirms that these exciplexes have predominantly CT excitations. This is consistent with the MOs for these excitations (*e.g.* HOMO–LUMO transition for toluene–TCNE 2A′, see Fig. S15, ESI†) and agrees with the ALMO-EDA results.

25202 | *Phys. Chem. Chem. Phys.*, 2024, **26**, 25192–25207

This journal is © the Owner Societies 2024

In conclusion, the analyses presented in this section complement the system-specific trends observed in the previous sections.

3.6 Averaged functional performance

To assess the overall performance of a TD-DFT method across all exciplexes, a mean absolute error (MAE) can be calculated as:

$$\mathrm{MAE} = \frac{\sum_{i=1}^{N} |y_i - x_i|}{N} \qquad (3)$$

where $|y_i - x_i|$ is the absolute error between y_i, the calculated TD-DFT value, and x_i, the reference value. A mean is obtained by summing each absolute error and dividing by N, the number of exciplexes. MAEs have been calculated in terms of D_e and r_e for the DFAs tested. The CT exciplexes (toluene–TCNE 2A′ and styrene-TMA) present unique challenges for TD-DFT as has been previously discussed. These exciplexes have been excluded from the present MAE discussion in order to facilitate an analysis of the averaged functional performance. The overall statistics for localised and CT exciplexes combined is provided in the ESI† (Section 7). Note that MAEs are primarily used here to provide a concise analysis of our results, despite the small sample size. That such numbers are nevertheless useful has been demonstrated for aromatic excimers before.[15]

3.6.1 Exciplexes with localised transitions. MAEs are shown in Fig. 12 for the exciplexes with a localised excitation, which are benzene–neon, benzene–argon, benzene–anthracene,

and toluene–TCNE 3A′. The unfilled bars show MAEs for the dispersion-uncorrected methods while the filled bars are for the D3(BJ)-corrected method where available. Methods which use the VV10 non-local kernel are shown with hatched bars. The tabulated values for MAE are provided in the ESI† When considering the dispersion-uncorrected methods, MAEs in D_e are generally reduced going up Jacob's ladder although this is not always the case. For example, the best performing GGA method is PBE which outperforms two global hybrid methods, B3LYP and BHLYP. Indeed, B3LYP has the worst performance of the tested global hybrids, consistent with ground-state benchmarking which has shown overall poor performance for this method despite its popularity.[10] The double-hybrid methods generally show the smallest errors, and of the dispersion-uncorrected methods the smallest MAE is 0.59 kcal mol^{-1} for SCS-RSX-QIDH.

RS reduces the MAEs for hybrid methods from an average of 5.19 kcal mol^{-1} to 3.28 kcal mol^{-1} Similarly, for the unscaled double-hybrids the averaged MAE reduces from 2.59 kcal mol^{-1} to only 1.60 kcal mol^{-1} with RS. Spin-scaling has a variable effect on the MAE for TD-DHDFAs. Each global double-hybrid shows an increased MAE when either SCS or SOS is applied. However, three of the RS double-hybrids are on average improved by spin-scaling (both SCS and SOS variants). These are RSX-QIDH, ωB88PP86, and ωPBEPP86. This is unsurprising for the latter two DFAs since spin-scaling was shown to counter the systematic overbinding for these methods.

For all DFAs tested, the ground-state D3(BJ) correction considerably reduces the MAE except for those RS double-hybrids for
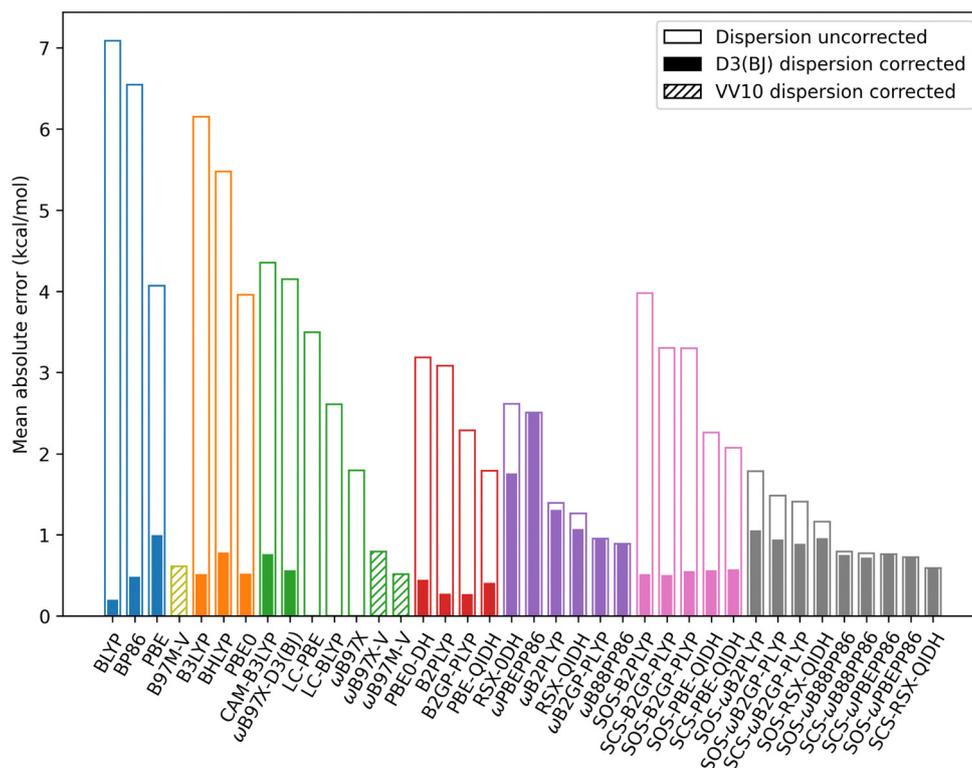

Fig. 12 MAEs for exciplexes with a localised excitation which are benzene–neon, benzene–argon, benzene–anthracene, and toluene–TCNE 3A′. MAEs are for D_e in kcal mol^{-1}.

which the dispersion correction has no impact. Overall, the dispersion-corrected method with the lowest MAE is BLYP-D3(BJ) with 0.20 kcal mol^{-1} error for D_e. This is followed closely by B2GP-PLYP-D3(BJ) (0.27 kcal mol^{-1} MAE) and B2PLYP-D3(BJ) (0.28 kcal mol^{-1} MAE). These MAEs outperform all of the dispersion-uncorrected methods. The strong performance of BLYP-D3(BJ) mirrors findings that this functional is competitive with double-hybrid accuracy for ground-state NCIs when tested on the S22 and S66 datasets.[10]

The VV10 dispersion-corrected methods generally have MAE's comparable, or slightly worse, compared to the D3(BJ)-corrected methods. B97M-V, which belongs to the meta-GGA rung on Jacob's ladder, is out-performed by two D3(BJ)-corrected GGAs but has a smaller MAE than PBE-D3(BJ). For the RS hybrid methods tested, MAEs are similar for VV10-corrected methods (ranging from 0.52 to 0.80 kcal mol^{-1}) compared to D3(BJ)-corrected methods (0.57 to 0.76 kcal mol^{-1}). Notably, ωB97X-D3(BJ) outperforms the original ωB97X-V functional by 0.23 kcal mol^{-1}. Of the VV10-corrected methods, ωB97M-V has the best performance with a MAE of 0.52 kcal mol^{-1}.

In terms of the equilibrium geometry r_e, trends to the MAEs are generally consistent with the observed trends for D_e. Going up Jacob's ladder and incorporating RS tend to decrease the MAE for r_e. However, MAEs are particularly large for the RS double-hybrid methods which have shown exciplex over-binding: ωB2GP-PLYP, ωB2PLYP, ωB88PP86, and ωPBEPP86. These methods predict a distance r_e which is considerably shorter than the reference. As before, the D3(BJ) correction greatly improves the calculated r_e except for the RS double-hybrids. When considering r_e, the best performing method is PBE-QIDH-D3(BJ) and the MAE is 0.03 Å. More details on the statistics for r_e can be found in the ESI.†

Finally, DFAs were assessed in terms of their performance for non-equilibrium geometries. In the spirit of the S66X8 data set,[11] 8 geometries were selected by scaling the equilibrium distance by multipliers which are: 0.90, 0.95, 1.00, 1.05, 1.10, 1.25, 1.50, and 2.00. That is, the dissociation curves were sampled at two compressed geometries, at the equilibrium geometry, and at 5 stretched geometries. The equilibrium distances were taken from the minima of the SCS-CC2/CBS(3,4) reference curves. The MAEs averaged over all non-equilibrium distances are given in the ESI.† Mean absolute percentage errors (MAPEs) were also calculated as per the original S66X8 analysis[11] and are also shown in the ESI.† From this analysis, B2PLYP-D3(BJ) has the smallest MAE which is 0.24 kcal mol^{-1}. The MAPEs generally yield similar trends, however the best method becomes PBE-QIDH-D3(BJ) (10% MAPE).

3.6.2 Exciplexes with CT excitations. For the CT exciplexes, toluene–TCNE (2A′) and styrene-TMA, MAEs are not evaluated. Instead, we provide a general analysis of TD-DFT methods for exciplexes with CT character. Firstly, for toluene–TCNE 2A′ the GGA and meta-GGA methods failed to predict the correct CT excitation. For styrene-TMA, these methods were associated with numerous ghost states and particularly large errors. This supports previous findings that (meta)-GGA methods should be

avoided in TD-DFT.[17,19,21,30,31] Further, the description of CT exciplexes shows pronounced improvement with the inclusion of RS. This is again in agreement with previous studies showing that RS is essential for calculating CT and other long-range excitations.[20,31,34,35] Considering both CT exciplexes, the RS TD-(SCS/SOS)-DHDFAs show the most robust performance. In particular, SOS-ωB88PP86 showed consistent good performance for these two exciplexes as did other RS TD-(SCS/SOS)-DHDFAs including ωB2(GP-)PLYP.

Exciplexes with a localised excitation showed near-universal improvement when a dispersion correction was included. This is not the case for the CT exciplexes. For styrene-TMA, the poor performance of the dispersion-corrected methods was shown to be a limitation of the underlying DFAs which over-bind this exciplex due to a redshifted CT excitation (see Section 3.2.2). The dispersion correction exacerbates overbinding for this exciplex. On the other hand, toluene–TCNE 2A′ shows improved performance when a dispersion correction is applied. However, the dispersion correction was insufficient to recover the true well-depth. The inconsistent behaviour of ground-state dispersion corrections for these exciplexes suggests that a state-specific dispersion correction is needed for robust performance with TD-DFT methods. These exciplexes further highlight the inherent limitations of current TD-DFT methods for long-range excitations.

4 Conclusions

In this study we have investigated excited-state non-covalent interactions (NCIs) in a series of dimers that consist of two different monomers with both older popular and more modern TD-DFT approaches. Accurate dissociation curves were calculated at the SCS-CC2/CBS(3,4) level of theory for five dimers with a total of six excited states. This reference method was used to benchmark a large number of DFAs which span the commonly-used rungs of Jacob's ladder and include RS methods and TD-SCS/SOS-DHDFAs. Additionally, we evaluated the performance of two ground-state dispersion corrections which are the DFT-D3(BJ) additive dispersion correction and the VV10 non-local kernel. Overall, the DFAs tested generally showed improved accuracy going up rungs of Jacob's ladder. GGA methods should be avoided in TD-DFT as these resulted in large errors, ghost excited states, and significant redshifts for CT excitation energies. For exciplexes with a localised excited state, GGA methods showed considerable under-binding and in some cases failed entirely to predict exciplex formation. Hybrid and double-hybrid DFAs reduced exciplex under-binding as did the RS methods.

Exciplexes with CT character proved particularly challenging for many of the assessed TD-DFT methods. For styrene-TMA, TD-DFT methods showed artificial over-binding due to redshifted excitation energies. The CT exciplexes required methods with a large proportion of non-local Fock exchange. Specifically, RS methods resulted in greatly improved accuracy for these exciplexes. CT exciplexes also benefitted

25204 | *Phys. Chem. Chem. Phys.*, 2024, **26**, 25192–25207

This journal is © the Owner Societies 2024

from TD-SCS/SOS-DHDFAs which were found to reduce exciplex binding compared to their unscaled counterparts.

In general, the ground-state DFT-D3(BJ) dispersion correction significantly improved the accuracy for all DFAs tested, except for RS TD-(SCS/SOS)-DHDFAs where D3(BJ) made little or no difference to the total energy. The other exception is styrene-TMA, which was already artificially over-bound and as such was not improved by a dispersion correction. The VV10 correction was also tested for the first time in the context of excited state NCIs and gave reasonably small errors comparable to D3(BJ)-corrected methods. The VV10 correction was also tested for its post-SCF implementation in its ground state, which resulted in no loss of accuracy and a reduced cost compared to self-consistent VV10. In fact, incorporating VV10 in the actual calculation of the excitation energies resulted to be negligible mirroring results previously reported in single-chromophore benchmarking.

Overall, the best performing TD-DFT methods for exciplex binding when only local excitations were involved were BLYP-D3(BJ), B2GP-PLYP-D3(BJ), and B2PLYP-D3(BJ). In particular, B2PLYP-D3(BJ) showed the best performance when non-equilibrium geometries were included. The latter two methods have previously shown excellent performance for excimer binding[15] and can be recommended for exciplexes. Despite its strong performance for localised excitations, BLYP-D3(BJ) is not recommended for TD-DFT due to its demonstrated inability to capture CT excitations and problems with ghost states. For the two CT exciplexes, dispersion-uncorrected SOS-ωB88PP86 gave the smallest errors, but ωB2(GP-)PLYP and a series of other RS TD-SCS/SOS-DHDFAs can also be recommended.

Finally, this study has reinforced that dispersion corrections are essential for good accuracy in (TD)-DFT calculations. While the D3(BJ) and VV10 dispersion corrections showed reduced errors, these did not reach chemical accuracy. In particular, the performance of the D3(BJ) correction was system- and method-dependent. We strongly recommend the development of a dispersion correction specifically for excited-state TD-DFT.

Author contributions

ACJ: conceptualization (equal), formal analysis (lead), investigation (lead), methodology (equal), validation (lead), visualization (lead), data curation (lead), writing – original draft (lead), writing – review & editing (equal). LG: conceptualization (equal), methodology (equal), formal analysis (supporting), investigation (supporting), funding acquisition (lead), project administration (lead), resources (lead), supervision (lead), writing – review & editing (equal).

Data availability

The data supporting this article have been included as part of the ESI.† Any raw data can be obtained from the corresponding author upon request.

Conflicts of interest

There are no conflicts to declare.

Acknowledgements

References

1 E. Runge and E. K. U. Gross, *Phys. Rev. Lett.*, 1984, **52**, 997–1000.

2 R. Bauernschmitt and R. Ahlrichs, *Chem. Phys. Lett.*, 1996, **256**, 454–464.

3 P. Hohenberg and W. Kohn, *Phys. Rev.*, 1964, **136**, B864–B871.

4 W. Kohn and L. J. Sham, *Phys. Rev.*, 1965, **140**, A1133–A1138.

5 F. London, *Z. Phys.*, 1930, **63**, 245–279.

6 S. Kristyán and P. Pulay, *Chem. Phys. Lett.*, 1994, **229**, 175–180.

7 J. M. Pérez-Jordá and A. D. Becke, *Chem. Phys. Lett.*, 1995, **233**, 134–137.

8 P. Hobza, J. Šponer and T. Reschel, *J. Comput. Chem.*, 1995, **16**, 1315–1325.

9 H. S. Yu, X. He, S. L. Li and D. G. Truhlar, *Chem. Sci.*, 2016, **7**, 5032–5051.

10 L. Goerigk, A. Hansen, C. Bauer, S. Ehrlich, A. Najibi and S. Grimme, *Phys. Chem. Chem. Phys.*, 2017, **19**, 32184–32215.

11 J. Řezáč, K. E. Riley and P. Hobza, *J. Chem. Theory Comput.*, 2011, **7**, 2427–2438.

12 J. Řezáč, K. E. Riley and P. Hobza, *J. Chem. Theory Comput.*, 2011, **7**, 3466–3470.

13 N. Mardirossian and M. Head-Gordon, *Mol. Phys.*, 2017, **115**, 2315–2372.

14 L. Goerigk and S. Grimme, *Phys. Chem. Chem. Phys.*, 2011, **13**, 6670–6688.

15 A. C. Hancock and L. Goerigk, *RSC Adv.*, 2023, **13**, 35964–35984.

16 M. R. Silva-Junior, M. Schreiber, S. P. A. Sauer and W. Thiel, *J. Chem. Phys.*, 2008, **129**, 104103.

17 D. Jacquemin, V. Wathelet, E. A. Perpète and C. Adamo, *J. Chem. Theory Comput.*, 2009, **5**, 2420–2435.

18 J. Liang, X. Feng, D. Hait and M. Head-Gordon, *J. Chem. Theory Comput.*, 2022, **18**, 3460–3473.

19 L. Goerigk and S. Grimme, *J. Chem. Phys.*, 2010, **132**, 184103.

20 M. Casanova-Páez, M. B. Dardis and L. Goerigk, *J. Chem. Theory Comput.*, 2019, **15**, 4735–4744.

This journal is © the Owner Societies 2024

Phys. Chem. Chem. Phys., 2024, **26**, 25192–25207 | **25205**

21 L. Goerigk, J. Moellmann and S. Grimme, *Phys. Chem. Chem. Phys.*, 2009, **11**, 4611–4620.

22 M. Véril, A. Scemama, M. Caffarel, F. Lipparini, M. Boggio-Pasqua, D. Jacquemin and P.-F. Loos, *Wiley Interdiscip. Rev.: Comput. Mol. Sci.*, 2021, **11**, 1517.

23 R. Grotjahn and M. Kaupp, *J. Chem. Phys.*, 2021, **155**, 124108.

24 A. D. Laurent and D. Jacquemin, *Int. J. Quantum Chem.*, 2013, **113**, 2019–2039.

25 C. Diedrich and S. Grimme, *J. Phys. Chem. A*, 2003, **107**, 2524–2539.

26 L. Goerigk and S. Grimme, *J. Phys. Chem. A*, 2009, **113**, 767–776.

27 K. Batra, S. Zahn and T. Heine, *Adv. Theory Simul.*, 2020, **3**, 1900192.

28 S. Grimme and F. Neese, *J. Chem. Phys.*, 2007, **127**, 154116.

29 M. Casanova-Páez and L. Goerigk, *J. Chem. Theory Comput.*, 2021, **17**, 5165–5186.

30 L. Goerigk and M. Casanova-Páez, *Aust. J. Chem.*, 2021, **74**, 3–15.

31 A. Dreuw, J. L. Weisman and M. Head-Gordon, *J. Chem. Phys.*, 2003, **119**, 2943–2946.

32 D. J. Tozer, R. D. Amos, N. C. Handy, B. O. Roos and L. Serrano-Andres, *Mol. Phys.*, 1999, **97**, 859–868.

33 D. J. Tozer, *J. Chem. Phys.*, 2003, **119**, 12697–12699.

34 A. Dreuw and M. Head-Gordon, *J. Am. Chem. Soc.*, 2004, **126**, 4007–4016.

35 M. Casanova-Páez and L. Goerigk, *J. Comput. Chem.*, 2021, **42**, 528–533.

36 L. Goerigk, H. Kruse and S. Grimme, *Comprehensive Chiroptical Spectroscopy*, Wiley-Blackwell, 2012, pp. 643–673.

37 T. Förster, *Angew. Chem., Int. Ed. Engl.*, 1969, **8**, 333–343.

38 M. Kołaski, C. R. Arunkumar and K. S. Kim, *J. Chem. Theory Comput.*, 2013, **9**, 847–856.

39 R. A. Krueger and G. Blanquart, *J. Phys. Chem. A*, 2019, **123**, 1796–1806.

40 R. Huenerbein and S. Grimme, *Chem. Phys.*, 2008, **343**, 362–371.

41 E. A. Briggs and N. A. Besley, *Phys. Chem. Chem. Phys.*, 2014, **16**, 14455–14462.

42 S. Grimme, *J. Comput. Chem.*, 2006, **27**, 1787–1799.

43 Y. Ikabata and H. Nakai, *J. Chem. Phys.*, 2012, **137**, 124106.

44 A. C. Hancock, E. Giudici and L. Goerigk, *J. Comput. Chem.*, 2024, **45**, 1667–1681.

45 S. Grimme, *J. Chem. Phys.*, 2003, **118**, 9095–9102.

46 Y. Jung, R. C. Lochan, A. D. Dutoi and M. Head-Gordon, *J. Chem. Phys.*, 2004, **121**, 9793–9802.

47 T. Schwabe and L. Goerigk, *J. Chem. Theory Comput.*, 2017, **13**, 4307–4323.

48 B. G. Janesko, T. M. Henderson and G. E. Scuseria, *J. Chem. Phys.*, 2009, **131**, 034110.

49 O. A. Vydrov, Q. Wu and T. van Voorhis, *J. Chem. Phys.*, 2008, **129**, 014106.

50 P. Mach, v Budzák, M. Medved' and O. Kysel', *Theor. Chem. Acc.*, 2012, **131**, 1268.

51 J. Van Dijk, M. Casanova-Páez and L. Goerigk, *ACS Phys. Chem. Au*, 2022, **2**, 407–416.

52 S. Grimme, J. Antony, S. Ehrlich and H. Krieg, *J. Chem. Phys.*, 2010, **132**, 154104.

53 S. Grimme, S. Ehrlich and L. Goerigk, *J. Comput. Chem.*, 2011, **32**, 1456–1465.

54 L. Goerigk and S. Grimme, *J. Chem. Theory Comput.*, 2011, **7**, 291–309.

55 M. Dion, H. Rydberg, E. Schröder, D. C. Langreth and B. I. Lundqvist, *Phys. Rev. Lett.*, 2004, **92**, 246401.

56 O. A. Vydrov and T. Van Voorhis, *J. Chem. Phys.*, 2010, **133**, 244103.

57 W. Hujo and S. Grimme, *J. Chem. Theory Comput.*, 2011, **7**, 3866–3871.

58 A. Najibi and L. Goerigk, *J. Chem. Theory Comput.*, 2018, **14**, 5725–5738.

59 A. Najibi, M. Casanova-Páez and L. Goerigk, *J. Phys. Chem. A*, 2021, **125**, 4026–4035.

60 O. Christiansen, H. Koch and P. Jørgensen, *Chem. Phys. Lett.*, 1995, **243**, 409–418.

61 A. Hellweg, S. A. Grün and C. Hättig, *Phys. Chem. Chem. Phys.*, 2008, **10**, 4119–4127.

62 F. Weigend and R. Ahlrichs, *Phys. Chem. Chem. Phys.*, 2005, **7**, 3297–3305.

63 *DFT-D3 V3.1*, S. Grimme, University of Bonn, 2014.

64 F. Neese, *Wiley Interdiscip. Rev.: Comput. Mol. Sci.*, 2012, **2**, 73–78.

65 F. Neese, *Wiley Interdiscip. Rev.: Comput. Mol. Sci.*, 2022, **12**, e1606.

66 J. P. Perdew and K. Schmidt, *AIP Conf. Proc.*, 2001, **577**, 1–20.

67 A. D. Becke, *Phys. Rev. A: At., Mol., Opt. Phys.*, 1988, **38**, 3098–3100.

68 C. Lee, W. Yang and R. G. Parr, *Phys. Rev. B: Condens. Matter Mater. Phys.*, 1988, **37**, 785–789.

69 B. Miehlich, A. Savin, H. Stoll and H. Preuss, *Chem. Phys. Lett.*, 1989, **157**, 200–206.

70 J. P. Perdew, K. Burke and M. Ernzerhof, *Phys. Rev. Lett.*, 1996, **77**, 3865–3868.

71 J. P. Perdew, *Phys. Rev. B: Condens. Matter Mater. Phys.*, 1986, **33**, 8822–8824.

72 N. Mardirossian and M. Head-Gordon, *J. Chem. Phys.*, 2015, **142**, 074111.

73 A. D. Becke, *J. Chem. Phys.*, 1993, **98**, 5648–5652.

74 P. J. Stephens, F. J. Devlin, C. F. Chabalowski and M. J. Frisch, *J. Phys. Chem.*, 1994, **98**, 11623–11627.

75 A. D. Becke, *J. Chem. Phys.*, 1993, **98**, 1372–1377.

76 C. Adamo and V. Barone, *J. Chem. Phys.*, 1999, **110**, 6158–6170.

77 M. Ernzerhof and G. E. Scuseria, *J. Chem. Phys.*, 1999, **110**, 5029–5036.

78 Y. Tawada, T. Tsuneda, S. Yanagisawa, T. Yanai and K. Hirao, *J. Chem. Phys.*, 2004, **120**, 8425–8433.

79 T. Yanai, D. P. Tew and N. C. Handy, *Chem. Phys. Lett.*, 2004, **393**, 51–57.

80 N. Mardirossian and M. Head-Gordon, *Phys. Chem. Chem. Phys.*, 2014, **16**, 9904–9924.

81 H. Iikura, T. Tsuneda, T. Yanai and K. Hirao, *J. Chem. Phys.*, 2001, **115**, 3540–3544.

25206 | *Phys. Chem. Chem. Phys.*, 2024, **26**, 25192–25207

This journal is © the Owner Societies 2024

82 J.-D. Chai and M. Head-Gordon, *J. Chem. Phys.*, 2008, **128**, 084106.

83 N. Mardirossian and M. Head-Gordon, *J. Chem. Phys.*, 2016, **144**, 214110.

84 A. Karton, A. Tarnopolsky, J.-F. Lamère, G. C. Schatz and J. M. L. Martin, *J. Phys. Chem. A*, 2008, **112**, 12868–12886.

85 S. Grimme, *J. Chem. Phys.*, 2006, **124**, 034108.

86 E. Brémond, J. C. Sancho-García, A. J. Pérez-Jiménez and C. Adamo, *J. Chem. Phys.*, 2014, **141**, 031101.

87 J. C. Sancho-García, E. Brémond, M. Savarese, A. J. Pérez-Jiménez and C. Adamo, *Phys. Chem. Chem. Phys.*, 2017, **19**, 13481–13487.

88 E. Brémond and C. Adamo, *J. Chem. Phys.*, 2011, **135**, 024106.

89 L. Goerigk and S. Grimme, *Wiley Interdiscip. Rev.: Comput. Mol. Sci.*, 2014, **4**, 576–600.

90 E. Brémond, A. J. Pérez-Jiménez, J. C. Sancho-García and C. Adamo, *J. Chem. Phys.*, 2019, **150**, 201102.

91 E. Brémond, M. Savarese, A. J. Pérez-Jiménez, J. C. Sancho-García and C. Adamo, *J. Chem. Theory Comput.*, 2018, **14**, 4052–4062.

92 M. Alipour and N. Karimi, *J. Chem. Theory Comput.*, 2021, **17**, 4077–4091.

93 E. Brémond, A. J. Pérez-Jiménez, J. C. Sancho-García and C. Adamo, *J. Chem. Phys.*, 2023, **159**, 234104.

94 S. G. Balasubramani, G. P. Chen, S. Coriani, M. Diedenhofen, M. S. Frank, Y. J. Franzke, F. Furche, R. Grotjahn, M. E. Harding, C. Hättig, A. Hellweg, B. Helmich-Paris, C. Holzer, U. Huniar, M. Kaupp, A. Marefat Khah, S. Karbalaei Khani, T. Müller, F. Mack, B. D. Nguyen, S. M. Parker, E. Perlt, D. Rappoport, K. Reiter, S. Roy, M. Rückert, G. Schmitz, M. Sierka, E. Tapavicza, D. P. Tew, C. van Wüllen, V. K. Voora, F. Weigend, A. Wodyński and J. M. Yu, *J. Chem. Phys.*, 2020, **152**, 184107.

95 E. Epifanovsky, A. T. B. Gilbert, X. Feng, J. Lee, Y. Mao, N. Mardirossian, P. Pokhilko, A. F. White, M. P. Coons, A. L. Dempwolff, Z. Gan, D. Hait, P. R. Horn, L. D. Jacobson, I. Kaliman, J. Kussmann, A. W. Lange, K. U. Lao, D. S. Levine, J. Liu, S. C. McKenzie, A. F. Morrison, K. D. Nanda, F. Plasser, D. R. Rehn, M. L. Vidal, Z.-Q. You, Y. Zhu, B. Alam, B. J. Albrecht, A. Aldossary, E. Alguire, J. H. Andersen, V. Athavale, D. Barton, K. Begam, A. Behn, N. Bellonzi, Y. A. Bernard, E. J. Berquist, H. G. A. Burton, A. Carreras, K. Carter-Fenk, R. Chakraborty, A. D. Chien, K. D. Closser, V. Cofer-Shabica, S. Dasgupta, M. de Wergifosse, J. Deng, M. Diedenhofen, H. Do, S. Ehlert, P.-T. Fang, S. Fatehi, Q. Feng, T. Friedhoff, J. Gayvert, Q. Ge, G. Gidofalvi, M. Goldey, J. Gomes, C. E. González-Espinoza, S. Gulania, A. O. Gunina, M. W. D. Hanson-Heine, P. H. P. Harbach, A. Hauser, M. F. Herbst, M. Hernández Vera, M. Hodecker, Z. C. Holden, S. Houck, X. Huang, K. Hui, B. C. Huynh, M. Ivanov, A. Jász, H. Ji, H. Jiang, B. Kaduk, S. Kähler, K. Khistyaev, J. Kim, G. Kis, P. Klunzinger, Z. Koczor-Benda, J. H. Koh, D. Kosenkov, L. Koulias, T. Kowalczyk, C. M. Krauter, K. Kue, A. Kunitsa, T. Kus, I. Ladjánszki, A. Landau, K. V. Lawler, D. Lefrancois and S. Lehtola, *et al.*, *J. Chem. Phys.*, 2021, **155**, 084801.

96 K. Eichkorn, O. Treutler, H. Öhm, M. Häser and R. Ahlrichs, *Chem. Phys. Lett.*, 1995, **242**, 652–660.

97 R. Izsák and F. Neese, *J. Chem. Phys.*, 2011, **135**, 144105.

98 F. Weigend and M. Häser, *Theor. Chem. Acc.*, 1997, **97**, 331–340.

99 F. Weigend, M. Häser, H. Patzelt and R. Ahlrichs, *Chem. Phys. Lett.*, 1998, **294**, 143–152.

100 M. Head-Gordon, R. J. Rico, M. Oumi and T. J. Lee, *Chem. Phys. Lett.*, 1994, **219**, 21–29.

101 Y. M. Rhee and M. Head-Gordon, *J. Phys. Chem. A*, 2007, **111**, 5314–5326.

102 S. Grimme, A. Hansen, J. G. Brandenburg and C. Bannwarth, *Chem. Rev.*, 2016, **116**, 5105–5154.

103 S. Grimme, *J. Comput. Chem.*, 2004, **25**, 1463–1473.

104 M. Friede, S. Ehlert, S. Grimme and J.-M. Mewes, *J. Chem. Theory Comput.*, 2023, **19**, 8097–8107.

105 E. Caldeweyher, C. Bannwarth and S. Grimme, *J. Chem. Phys.*, 2017, **147**, 034112.

106 E. Caldeweyher, S. Ehlert, A. Hansen, H. Neugebauer, S. Spicher, C. Bannwarth and S. Grimme, *J. Chem. Phys.*, 2019, **150**, 154122.

107 N. Mehta, M. Casanova-Páez and L. Goerigk, *Phys. Chem. Chem. Phys.*, 2018, **20**, 23175–23194.

108 T. Risthaus and S. Grimme, *J. Chem. Theory Comput.*, 2013, **9**, 1580–1591.

109 Q. Ge, Y. Mao and M. Head-Gordon, *J. Chem. Phys.*, 2018, **148**, 064105.

110 F. Plasser and H. Lischka, *J. Chem. Theory Comput.*, 2012, **8**, 2777–2789.

This journal is © the Owner Societies 2024

Phys. Chem. Chem. Phys., 2024, **26**, 25192–25207 | **25207**